Electron energy distribution function in a pulsed 2.45GHz hydrogen magnetoplasma: Study of the decay

Jean-Louis Jauberteau, Isabelle Jauberteau, Daniel Osvaldo Cortazar, Ana Maria Megia-Macias

Electron energy distribution function in a pulsed 2.45GHz hydrogen magnetoplasma: Study of the decay

J. L. Jauberteau, I. Jauberteau, O. D. Cortázar, and A. Megía-Macías

Citation: AIP Advances **7**, 125107 (2017);
View online: https://doi.org/10.1063/1.5001271
View Table of Contents: http://aip.scitation.org/toc/adv/7/12
Published by the American Institute of Physics

Electron energy distribution function in a pulsed 2.45GHz hydrogen magnetoplasma: Study of the decay

J. L. Jauberteau,[1,a] I. Jauberteau,[1] O. D. Cortázar,[2] and A. Megía-Macías[3]
[1]*UMR 7315 CNRS, SPCTS, 12 rue Atlantis, 87068 Limoges, France*
[2]*Universidad de Castilla-La Mancha, ETSII-INEI, Av. Camilo Jose Cela s/n, 13071 Ciudad Real, Spain*
[3]*Department of Industrial Technologies, Faculty of Engineering, University of Deusto, Av. Universidades, 24, 48007 Bilbao, Vizcaya, Spain*

(Received 23 August 2017; accepted 24 November 2017; published online 8 December 2017)

This work is devoted to the study of the Electron Energy Distribution Function (EEDF) during the decay (afterglow) of a pulsed magnetoplasma working at 2.45GHz in H_2. The experiments are performed under resonance (B=0.087T) and off resonance (B=0.120T) conditions, at low (0.38Pa) and high pressure (0.62Pa) for incoming power ranging from 300W to 1500W. At steady state i.e. before the discharge decay, the EEDF profile exhibits three main components of which amplitude changes under experimental conditions. A low energy component (ε_e<10eV) is observed whatever experimental conditions are. An intermediate energy component is observed at energy ranging from 5eV to 15eV under resonance conditions. A high energy component is observed up to 30eV in the EEDF tail, mainly under off resonance conditions. Standard fitting methods are used to study the change of the different EEDF components versus time during afterglow. We show that the three components stand for different times: The low and high energy component stand from 10μs to 15μs and the intermediate energy component stands for only 5μs. The different decay characteristic times are discussed and the results are correlated to the electron recombination processes in the discharge, to the reminiscent incoming power observed up to 30μs, and to the peak observed in the reflected power during decays. We show that the low energy component decay is due to the electron recombination process, which is limited by the charge transfer process which produces H_3^+. https://doi.org/10.1063/1.5001271

I. INTRODUCTION

The study of transient physical phenomena in a pulsed magnetoplasma is of great interest for scientific and technological purposes and is important to develop new plasma techniques or to improve plasma applications, like ion sources, surface treatment reactors or propulsion magnetoplasma rockets.[1–5]

Transient phenomena during breakdown and decay of pulsed plasmas can be investigated using time resolved optical emission spectroscopy or Langmuir probe diagnostics. These efficient diagnostic methods have already been carried out to study the change of plasma parameters, discharge profile or emission intensity in hydrogen ECR plasmas.[6,7] In a previous work, we have studied the Electron Energy Distribution Function (EEDF) by means of time resolved Langmuir probe diagnostics, during the breakdown until the steady state of pulsed magnetoplasma working in hydrogen.[8] This study has been performed under Electron Cyclotron Resonance (ECR) and off resonance conditions. We have shown that the EEDF profile is composed of three main components, depending on experimental conditions. A first low energy component is observed at electron energy lower than 10eV which

[a]E-mail: jean-louis.jauberteau@unilim.fr

is due to the inelastic collision processes between electrons and neutrals (mainly H_2). A second intermediate energy component is observed under ECR conditions (B=0.087T). This component is detected at electron energy ranging from 5eV to 15eV, with a peak at about 10eV. Such EEDF distortion has been observed by Takashi et al[9] in hydrogen plasma working at 8MHz and 4KW and has been ascribed to the formation of a standing wave in the plasma.

The third component is a Maxwell-Boltzmann distribution and corresponds to the tail of the EEDF. This component is lower than the two former and is hidden by the intermediate energy component under resonance conditions. Consequently, it is mainly observed under off resonance conditions.[8]

The purpose of this work is to investigate the plasma decay after pulse which corresponds to an afterglow already observed in ECR ion sources.[10,11] This plasma decay has been previously clearly detected in the incoming and reflected power signal and in the electron temperature evolution.[12]

This work comes after the previous one devoted to the study of breakdown and steady state observed in pulsed microwave plasma. At first we study the time evolution of the three main EEDF components during off time. The results are correlated to those given in previous publications.[8–12] Then, we discuss the characteristic decay time corresponding to each component which is correlated to the electron kinetic during afterglow.

For the sake of clarity, the terms of low, intermediate and high energy components are used for energy ranging from 0 to 10eV, 5 to 15 eV and up to 30eV, respectively, although the terms of intermediate and high energy component usually correspond to KeV and ten or hundred of KeV, respectively.

II. EXPERIMENTAL SET-UP

The experimental set-up has been described in previous publications.[12–14] The apparatus consists of a cylindrical vessel made in oxygen free copper with 93mm length (z-axis) and 90mm diameter (r-axis). A set of four coaxial coils arranged in four pancakes with adjustable current and positioning mechanism produces a magnetic field profile oriented according to the longitudinal axis. The plasma generator is driven by a 3KW adjustable power magnetron of 2.45GHz operating at 100Hz in pulsed mode with a duty cycle of 50%. Time resolved Langmuir probe measurements have been performed within the reactor. The probe is a tungsten wire (6mm length and 0.5mm diameter), located in the middle of the plasma chamber (at r=0mm and z=46mm). The Langmuir probe is driven by an ESPION system (Hiden analytical LTD). When the synchronization is carefully made, the measurements are carried out at an accurately defined moment with respect to the beginning of the incoming power signal with a temporal resolution of 200ns.[12] Modifying the trigger delay, a set of I-V probe characteristics can be obtained during the decay. The best results are obtained by averaging 20 data acquisitions for each point, performed in different consecutive pulses to account for pulses reproducibility and noise.

The incoming and reflected signals are measured with a bi-directional coupler, calibrated for 2.45GHz which gives information on the incident and reflected power of the microwave versus time.

EEDF profiles is calculated using a home made data treatment software based on the Arslanbekov theory to correct the effect of the magnetic field on the electron current branch of the IV probe characteristic.[15] The second derivatives of I-V probe characteristics are calculated using the numerical Simulation of Harmonic Component (SHC) method.[17] Data treatments and magnetic field correction methods have been already published and are not detailed in this paper. We just give the main lines concerning the EEDF corrections in a magnetic field. The present work is mainly focused on the behaviour of the different EEDF components during afterglow.

A. Conditions to measure undisturbed EEDF

We first remember the condition necessary to measure undisturbed EEDF by means of Langmuir probes. The undisturbed EEDF is formed along a length of order of the electron energy relaxation length λ_ε. So, the region disturbed by the probe should have a length r_d much lower than the electron energy relaxation length, if we want to have any information about the undisturbed EEDF of the

bulk plasma. When the condition $\lambda_\varepsilon >> r_d$ is fulfilled, one can neglect the electron energy change in collisions and heating by the external electric field and consider in the electron kinetic equation only the diffusion term due to the space gradient produced around the probe.[15] When the condition $\lambda_\varepsilon >> r_d$ is not fulfilled, the probe characteristic loses most of its information about the undisturbed EEDF of the plasma bulk which cannot be measured. Because of the magnetic field, the charged particles rotate within the plasma along the magnetic field according to a spiral with radius equal to the Larmor radius. Because of the mass difference between ions and electrons, and the low magnetic field (0.087T-0.12T), only the electron trajectory is affected. The ion motion remains nearly unchanged. In the presence of the magnetic field, the electron diffusion is a tensor with two components in the directions parallel and perpendicular to the magnetic field, respectively. The electron kinetic equation has also the form of the anisotropic diffusion equation.[15] The electron collision frequency increases and the electron energy relaxation length decreases with increasing magnetic field.[18]

In a previous work,[8] the electron relaxation length in hydrogen plasma has been calculated using the total electron collision cross section given by Tawara et al,[19] which includes elastic and inelastic collisions of electrons with H_2, and inelastic collisions of electron with H, H^+, H_2^+, H_3^+ (recombination processes). Figure 1 shows the change of the ratio of the electron relaxation length to the probe disturb length given by $r_d = r_p \ln(L/r_p) = 7.3\text{x}10^{-4}\text{m}$,[15] versus electron energy up to 60eV. At low electron energy (<1eV), the electron energy relaxation length depends mainly on the electron-ion collisions and the ratio λ_ε/r_d depends on the ion density. The electron-ion recombination cross section depends on the vibrational and rotational level of the ion excited state. Assuming that the main ions are H_2^+(v=0,1,2) and that T_i=1160K (ε_i=0.1eV), the ratio λ_ε/r_d is lower than 1 for electron energy lower than 0.2eV when the electron density is $1\text{x}10^{17}\text{m}^{-3}$ and for electron energy lower than 0.05eV when the electron density equals to $1\text{x}10^{16}$ m^{-3}.

Then the ratio increases with electron energy increasing up to 14 at 10eV. At electron energy larger than the electron-neutral inelastic collision threshold (between 10eV and 16eV), the ratio drastically decreases up to 2.15 at 16eV because of the successive inelastic collision processes like the $B^3\Sigma_u^+$, $C^1\Pi_u$ and $B^1\Sigma_u^+$ electronic state excitations then the ionization of H_2. At larger electron energy, the ratio slowly decreases with electron energy increasing and becomes lower than 1 at about 30eV. It is worth noting that for electron energy larger than 1eV, the electron energy relaxation length depends mainly on the electron-neutral collisions, molecular hydrogen being the main neutral species in plasma. As previously written,[8] these results are calculated considering the radial components of the electron energy relaxation length. In the direction parallel to the magnetic field, the energy relaxation length is 2 or 3 orders of magnitude larger than the value obtained in the case of the radial component.

It can be seen that the probe disturbed length is smaller than the electron relaxation length for most of electrons produced in the plasma. So we will assume that the EEDF measured is a non-local distribution representative of the plasma bulk. As previously explained, in this case the electron

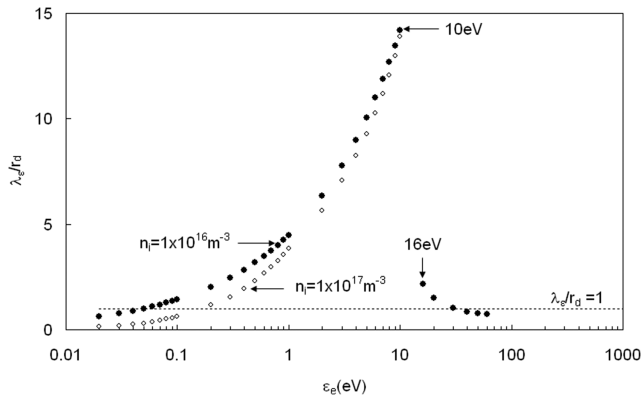

FIG. 1. Ratio of the electron energy relaxation length (radial component) to the disturbed probe length versus electron energy up to 60eV, in H_2 magnetoplasma. In the case of the electron-ion collisions, calculations have been done assuming an ion density equal to $1\text{x}10^{16}\text{m}^{-3}$ and $1\text{x}10^{17}\text{m}^{-3}$. The straight line indicates the ratio equal to 1.

kinetic equation depends only on the diffusion term through the probe disturbed length. Because the magnetic field has an effect on the diffusion term, a correction of the IV probe characteristic is necessary.

B. The correction method

The theory of magnetized plasma has been developed for electrostatic probe in a non-local approach when electron reach the probe in a diffusion regime i.e. when $\lambda_\varepsilon >> r_d$.[15,16] The method used in the work to determine the EEDF has already been detailed in the previous works.[8] We just remember in this article the main lines of the method used.

It can be shown that the electron current collected depends on a diffusion parameter $\psi(\varepsilon_e)$ and can be written,[15,16]

$$I_e(U) = \frac{8\pi eS}{3m^2\gamma}\int_{eU}^{\infty}\frac{(\varepsilon_e - eU)f(\varepsilon_e)d\varepsilon_e}{1+((\varepsilon_e - eU)/\varepsilon_e)\Psi(\varepsilon_e)} \tag{1}$$

Where, ε_e is the total electron energy in the sheath, U is the probe potential with respect to the plasma potential, $\psi(\varepsilon_e)$ is the diffusion parameter depending on ε_e, S is the collecting probe area, γ is a geometric factor varying monotonically from 0.71 when the Larmor radius $\rho_e << r_s$ (the sheath radius) to 4/3, when $\rho_e >> r_s$.[15] $f(\varepsilon_e)$ is the isotropic EEDF given by,

$$\int_0^{\infty} f(\varepsilon_e)\sqrt{\varepsilon_e}d\varepsilon_e = n,$$

n is the electron density. In the present case, considering the cylindrical probe placed parallel to the magnetic field, the diffusion parameter is given by,[16]

$$\Psi = \frac{\pi L}{4\gamma\rho_e} \tag{2}$$

This factor depends on the electron energy and on the magnetic field. It doesn't depend on the electron mean free path. In the absence of a magnetic field, the diffusion parameter equal 0 and Equation (1) is simplified and corresponds to the classical regime in the absence of magnetic field and at low pressure,

$$I_e(U) = \frac{2\pi eS}{m^2}\int_{eU}^{\infty}(\varepsilon_e - eU)f(\varepsilon_e)d\varepsilon_e \tag{3}$$

The second derivative of the electron current in presence of a magnetic field is calculated using Equation (1) and is given by,

$$I''(U) = Cf(eU) - C\int_{eU}^{\infty}K(\varepsilon_e, U)f(\varepsilon_e)d\varepsilon_e \tag{4}$$

Where $C = \frac{e^3 A_p}{2\gamma\sqrt{2m_e}}$ (Ap is the probe area) and

$$K(\varepsilon_e, U) = \frac{2\Psi{\varepsilon_e}^2}{[\varepsilon_e(1+\Psi) - \Psi eU]^3}$$

The first term of the right side in the equation is the Druyvesteyn formula and the second one describes the effect of the electron depletion around the probe, depending on the diffusion parameter. The method used to determine the EEDF profile from the second derivative of the probe characteristics has been detailed in the previous work[8] and will not be discussed anymore in this article. It can be summarized as follows: First the EEDF is calculated using the Druyvesteyn equation and second by means of successive adjustments of the previous distribution function, we correct the EEDF in order to obtain a perfect agreement between the experimental second derivative and the calculated one using Equation (4). In these conditions, the EEDF obtained is solution of Equation (4) and the correction of the EEDF taking into account the effect of the magnetic field on the diffusion through the probe disturbed region is done all over the electron energy range. The integral part of Equation (4) is calculated by means of a Monte Carlo integration method. It is worth noting that equation (4) shows that the EEDF is proportional to the second derivative of the I-V probe characteristic in the retarding region only if the second term of the equation (the integral term) can be neglected compared to the

first one. This means that the plasma potential can be measured at the zero crossing point of the second derivative with the x-axis only if the second term in Equation (4) (the integral part) can be neglected when the probe is biased at the plasma potential. In the previous work,[8] we have shown that for U close to 0, this approximation is available in these experiments and the determination of the plasma potential at the zero crossing point of the second derivative is available.

The electron density has been determined using two different methods. First in a previous work, using the electron current measured when the probe is biased at the potential plasma V_p.[12] Second in this work, integrating over the total EEDF after correction of the magnetic field effect i.e. measured using the present method. The electron density measured using the first method gives values ranging from $1x10^{16}$ to $3x10^{16}$ m^{-3} according the experimental condition. Using the second method an increase of the electron density from 20% to 100% is observed compared to the previous method. This is due to the correction of the effect of the magnetic field on the collected electron current which is not taken into account in the first method. Frequently in magnetic plasma, electron densities are measured using the ion current at saturation. This method is available as long as a) the magnetic field has no effect on the ion motion, b) there is the continuity of the ion flow through the probe sheath (collisionless condition for ion in the sheath) and c) the EEDF is a Maxwell-Boltzmann distribution.[20] Concerning this last point, Vasil'Eva has shown that in non maxwellian plasma the ion probe current depends on the EEDF shape and that changes which lead to a sharper drop in electron density in the repulsive field of the probe sheath decrease the collected ion current.[21] In our experiments, the ion current continuity and the maxwellian EEDF conditions are not fulfilled. So we cannot use this last method to measure the electron density. For information it would give electron density ranging from $1x10^{17}m^{-3}$ to $3x10^{17}m^{-3}$.

Using the derivative of Equation (1) and (3) with respect to ε_e, it can be shown that at saturation (i.e. when U=0), the ratio of the derivative of the electron current measured with (I_e) and without (I_0) magnetic field is given by,

$$\frac{dI_e(\varepsilon_e)}{dI_0(\varepsilon_e)} = \frac{4}{3\gamma}(1 + \Psi(\varepsilon_e))^{-1}. \tag{5}$$

$\Psi(\varepsilon_e)$ is given by Equation (2) and can be approximated by $\Psi(\varepsilon_e) = \frac{1500B}{\sqrt{\varepsilon_e}}$, where B is the magnetic field in Tesla unit and ε_e, the electron energy is in eV. When B=0, $\rho_e >> r_s$, γ=4/3 and $dI_e(\varepsilon_e) = dI_0(\varepsilon_e)$.

Considering the space-charge limited current, Dote et al[22] have shown that the electron current at saturation, depends on the angular cyclotron frequency (ω), on the mean collision time between electrons and molecules (τ) and on the mean free path of electron (λ_e). They show that only one part of the electron current at saturation measured in the absence of magnetic field (Io) is collected when a magnetic field is applied and,

$$I_0 = I_e\left(1 + C\frac{\left(1+\omega^2\tau^2\right)^{1/2}}{\lambda_e}\right) \tag{6}$$

I_0 and I_e are the electron currents at saturation measured without and with magnetic, respectively. C is a constant, depending on the probe geometry. In this equation the term $I_e C\frac{(1+\omega^2\tau^2)^{1/2}}{\lambda_e}$, corresponds to the electron current lost because of the electron gyration in the magnetic field. For electron energy ranging from 0.01ev to 10eV, the electron mean free path ranges from $4x10^{-2}$m to $2.6x10^{-2}$m and the mean collision time ranges from $4.7x10^{-7}$s to $1.4x10^{-8}$s. At an angular cyclotron frequency of 2.45GHz (resonance condition), the product $\omega\tau >> 1$ and the ratio I_e/I_0 calculated using Equation (6) can be approximated by,

$$\frac{I_e}{I_0} = \left(1 + C\frac{\omega\tau}{\lambda_e}\right)^{-1} = \left(1 + C\frac{1}{\rho_e}\right)^{-1} = \left(1 + C'\frac{B}{(\varepsilon_e)^{1/2}}\right)^{-1} \tag{7}$$

Where C' and B are a constant and the magnetic field.

It can be seen that when $\omega\tau >> 1$, Equation (7) obtained using Dote theory[22] and Equation (5) obtained using Arslanbekov theory[15,16] depend on B and ε_e and not on other parameters like neutral or charged particles density or e-neutral or e-ion collision cross section. Figure 2 shows the ratio

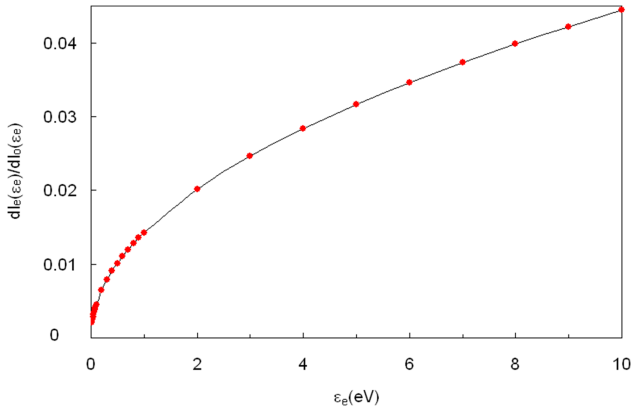

FIG. 2. $\frac{dI_e(\varepsilon_e)}{dI_0(\varepsilon_e)}$ versus electron energy, determined at B=0.087T.

$\frac{dI_e(\varepsilon_e)}{dI_0(\varepsilon_e)}$ versus the electron energy calculated using Equation (5) in the case of B=0.087T. Same result is obtained using Equation (7). The ratio increases with ε_e increasing, from $2.0\text{x}10^{-3}$ to $1.4\text{x}10^{-2}$ for ε_e equal to 0.02eV and 1eV, respectively. Then at 10eV, it is equal to $4.4\text{x}10^{-2}$. So, when a magnetic field is applied the electron current branch of the IV probe characteristic is reduced. This is due to the change of the diffusion parameter $\psi(\varepsilon_e)$ in the Arslanbekov theory[15] or to the change of $\frac{\omega\tau}{\lambda_e}$ in the Dote theory.[22] Both parameters depends on B and ε_e only. The method used in the present work to determine the EEDF (Equation (4)) takes into account the correction of the electron current reduced because of the applied magnetic field. It is worth noting that the plasma heating of ions by electron-ion collisions and thus also heating of neutral by ion-neutral collisions could reduce the neutral density. However, this change will have no effect on the diffusion coefficient $\psi(\varepsilon_e)$ or on $\frac{\omega\tau}{\lambda_e} = \frac{1}{\rho_e}$ and consequently on the electron part of the probe current.

Nevertheless, the energy relaxation length can be increases when electron-neutral collisions are dominant because of the change in collision frequency. This reduce the effect of the probe disturb region on the EEDF measured.

C. The magnetic field profile within the reactor

The investigations have been performed when the probe is located in a plasma region under resonance and off resonance conditions, with a magnetic field equal to 0.087T ($B=B_{ECR}$) and 0.12T ($B>B_{ECR}$), respectively. Figure 3 shows the magnetic profiles obtained with experimental validated simulations. Notice the position of the ECR surface and Langmuir probe. These configurations correspond to more or less homogeneous magnetic field along the reactor axis in the part where the probe is located.

Under off resonance conditions, there is a diverging B field with $B>B_{ECR}$ for a large part of the volume. The magnetic field increases on the reactor axis with increasing z-axis: B=0.110T at z=40mm and it ranges from 0.120T to 0.126T for z value larger than 45mm up to the end of cavity. On the left side (see Figure 3) there is ECR resonance condition. This corresponds to a one side resonance condition. So the plasma is still made at the resonance condition but the probe is located in a no resonance region. For this condition only the higher pressure gives good results.

Under off resonance condition, the gradient in magnetic field within the reactor could cause a situation with larger flows and thus lower densities. So, plasma is probably not homogeneous along the z axis from z=20mm up to 80mm (see FIG.3b).

Under resonance condition, the magnetic field has a symmetric profile which is constant and equal to about 0.087T from z=15mm to 80mm.[12]

III. RESULTS AND DISCUSSION

Figure 4 compares the EEDF measured at a power of 1500W and pressures of 0.38Pa (LP) and 0.62Pa (HP), both under resonance and off resonance conditions (one side resonance condition).

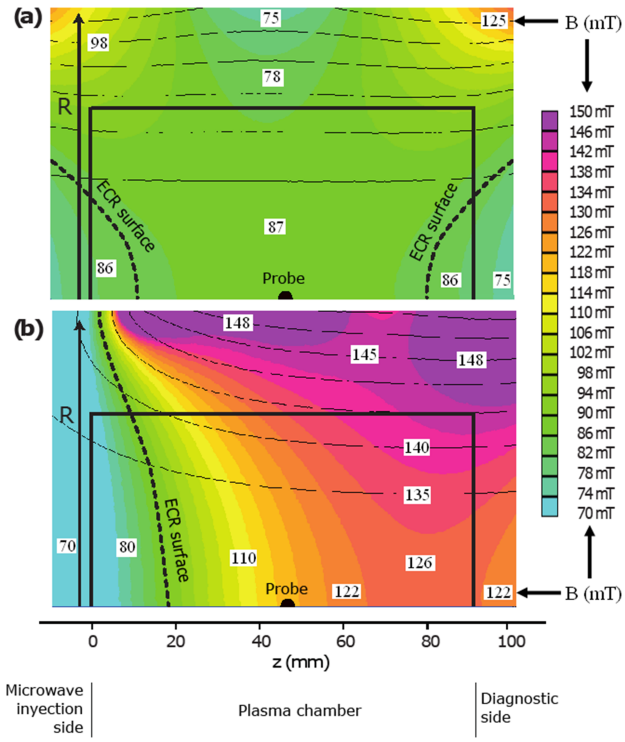

FIG. 3. Views of the magnetic field profiles used during experiments. Black solid lines represent the plasma chamber volume and dashed lines the position of the ECR surfaces. Subfigure (a) corresponds to 0.087T ($B=B_{ECR}$) and (b) to 0.12T ($B>B_{ECR}$). The position of the Langmuir probe is indicated by the black dot. In the white inserts are indicated some local B values in mT.

It can be seen that the lowest EEDF profile is obtained at low pressure under off resonance conditions and the highest EEDF at low pressure under resonance conditions. In this case, the EEDF profile exhibits a strong intermediate energy component between 5eV and 15eV, which is vanished when B=0.12T (off resonance). It must be noticed that the results obtained at low pressure and B=0.12T are generally strongly disturbed because of the low signal so we do not use these results. The low energy component, observed at $\varepsilon_e<10$eV, increases with increasing pressure i.e. increasing electron-neutral collision frequency.

The intermediate energy component appears at B=0.087T, when the incoming power is larger than 600W. It becomes the main component at 1500W. At B=0.12T, this component disappears and a

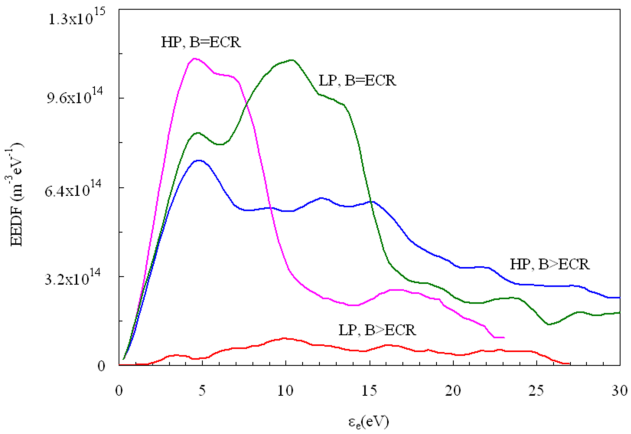

FIG. 4. EEDF measured under different experimental conditions: at 1500W, low pressure (LP) and high pressure (HP), under resonance and off resonance conditions.

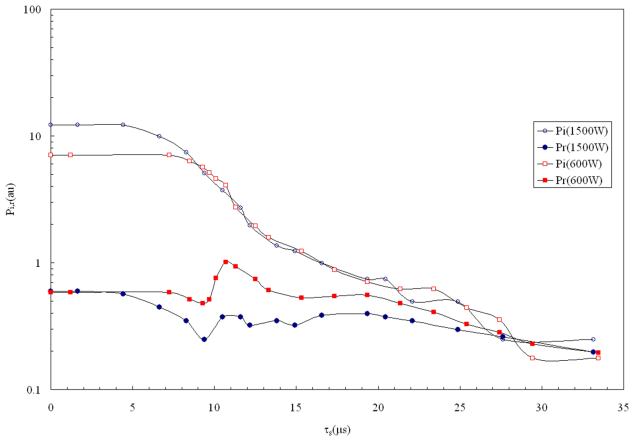

FIG. 5. Incoming (P_i) and reflected (P_r) microwave signal measured during the decay for a discharge working at 1500W and 600W, at 0.38Pa and under resonance conditions. The reflected power from plasma is ten times amplified with respect to the incoming power.

small and broad component corresponding to a Maxwell-Boltzmann distribution (T_e=19eV) is mainly observed in the tail of the distribution. It corresponds to electrons excited by the microwave which have not lost their energy in inelastic collisions with heavy particles. This last component is smaller than the two other ones, and is mainly observed under off resonance conditions.

The following part of the work is devoted to the behaviour of these three energy components during the afterglow. Figure 5 shows the change of the incoming and reflected microwave signal measured during the decay at 0.38Pa under ECR conditions, when the incoming power is equal to 1500W and 600W, respectively. The discharge is switched off between t=5μs and t=8μs, which corresponds to the start of the incoming power decay. In Figure 5, the incoming power signal is observed up to 25μs after the discharge is switched off. It decreases nearly exponentially versus time. The remaining incident power is about 40% to 50% of the initial incident power 5μs after switching off. The reflected power signal drops at the beginning of the decay then it rebounds. It consists of one or two peaks between 10μs and 20μs. This increase is more or less important depending on the experimental conditions. The magnetron produces 100Hz output in square pulses and the afterglow reflected signal peaks are not observed without the presence of plasma or by switching off the magnetic field. So, this is not due to the magnetron working.

Such behaviour is also observed at B=0.12T, and under other experimental conditions and can be correlated to the afterglow produced after switching off.[6,12] The exponential decay of the incoming power can be correlated to the microwave resonance within the cavity at 2.45GHz, produced during the off time. In previous works,[23] the coupling parameter of the reactor defined as, $\beta = \frac{1 \mp \sqrt{P_r/P_i}}{1 \pm \sqrt{P_r/P_i}}$ has been studied. This parameter is interesting because of its relationship with the quality factor. This study has shown that β strongly depends on experimental conditions and drastically changes with the electron density. A discrepancy of magnitude up to 2 on the coupling parameter value is measured when the discharge is on, compared to measurements performed in the empty cavity.[23] Such behaviour is expected for the quality factor which also strongly depends on the electron density changing versus time during afterglow.

In the following part of the paper, we define two times, τ_s and τ_d, corresponding to the beginning of the measurement and to the beginning of the decay, respectively. In the case of Figure 5, $\tau_d=(\tau_s - 5)$μs at 1500W and $\tau_d=(\tau_s - 8)$μs at 600W.

Figure 6–7 show the decay of the EEDF profile under ECR conditions at 1500 W at low and high pressures, respectively. The observations are performed from τ_s=0μs to 18μs. At low pressure, the EEDF shape changes just after switching off (τ_s=4-5μs). As shown on Figure 6, the intermediate energy component slightly moves to low energy and decreases with increasing low energy component. The low energy component decreases when the intermediate energy component is vanished at about τ_s=10μs i.e. τ_d=5μs and stands until τ_d=10μs-11μs after the switching off. The same behaviour is

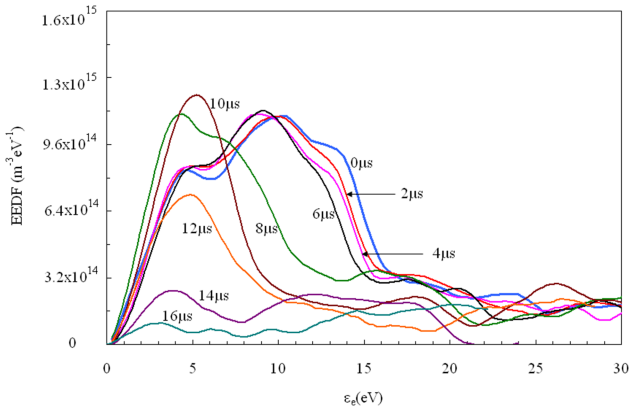

FIG. 6. Time evolution of EEDF measured at 0.38Pa and 1500W under resonance conditions.

observed under ECR conditions at high pressure (Figure 7). However in this case, the low energy component remains higher than at low pressure. On the figure, both low and intermediate energy components decrease up to τ_s=8µs (start of the incoming power decay), then, as previously, the intermediate energy component decreases with increasing low energy component until τ_s=12µs. For longer time, the low energy component decreases when the intermediate energy component is vanished, and disappears at about τ_s =18µs.

It is worth noting that the transient phenomenon observed between τ_s=8 to 12µs on figures 6 and 7, and corresponding to the decrease and increase of the intermediate and low energy components, respectively, can be correlated to the reflected power peak observed on Figure 5 and described in previous works.[12]

Figure 8 shows the EEDF decay measured at high pressure under off resonance conditions. The EEDF profile is lower than previously. It consists with low and high energy components (Maxwell-Boltzmann at Te=19eV), no intermediate energy component is observed. This one is not observed when the probe is located in a region of non resonance. It is correlated to the resonance conditions. The EEDF remain nearly unchanged up to τ_s=5-6µs which corresponds to the beginning of decays. Then, the low electron energy component increases with decreasing high electron energy component until τ_s=8µs. For longer times, both components simultaneously decrease and vanish at about τ_s=18µs.

A. The behavior of the three components during the plasma decay

In what follows, we study the decay process of each of these components under different experimental conditions. The EEDF profile has been decomposed in three main components using analytical functions.

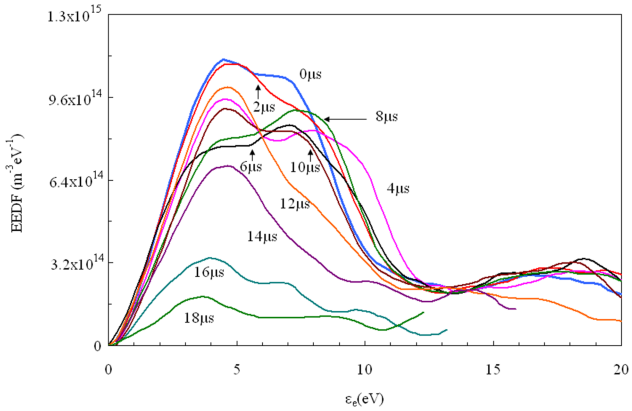

FIG. 7. Time evolution of EEDF measured at 0.62Pa and 1500W under resonance conditions.

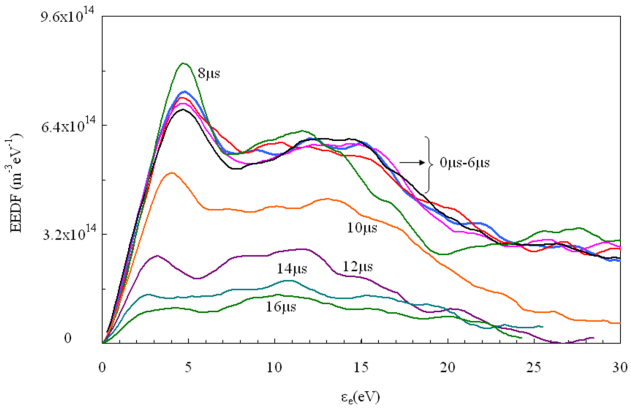

FIG. 8. Time evolution of EEDF measured at 0.62Pa and 1500W under off resonance conditions (B>ECR).

The low energy component is fitted using the function given by,

$$f(\varepsilon_e) = C_0\sqrt{\varepsilon_e}\exp(-(b\varepsilon_e^2 + c\varepsilon_e)\ln(\varepsilon_e)). \tag{8}$$

Where, *b, c, C_0* are constant values of real types. This function differs from the generalized Maxwell-Boltzmann distribution used in ref 8. It is more appropriated to fit the low energy part of the EEDF curve obtained under ECR conditions.

The tail of the EEDF curve is fitted to a Maxwell-Boltzmann distribution and the intermediate energy component is deduced removing the two former components from the total experimental EEDF measured.

Figure 9–10 show EEDF profiles decomposed in the different components, in the case of measurements performed at low pressure, 1500W for τ_s=1µs and τ_s=10µs, respectively and under resonance conditions. The discharge is switched off at τ_s=5µs. So, Figure 9 corresponds to the steady state and Figure 10 corresponds to τ_d=5µs after starting the decay.

The two figures show:

The low energy component C corresponding to b=0.07 and c=-0.55, the Maxwell-Boltzmann component B with Te=19eV, the sum (B+C) and the intermediate energy component deduced from the experimental EEDF i.e. (EEDF-sum(B+C)).

It can be seen on Figure 10 that the intermediate energy component is nearly vanished at τ_s=10µs (i.e. τ_d=5µs) whereas the Maxwell-Boltzmann component is decreased but it is not vanished at the same time.

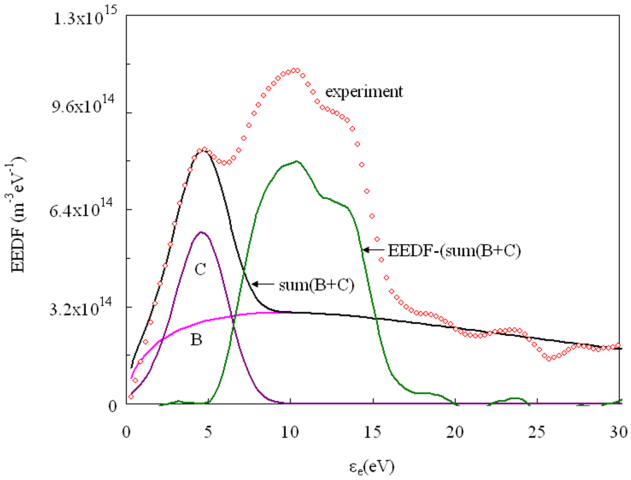

FIG. 9. Decomposition of EEDF in three main components; measurements are performed at low pressure at 1500W and τ_s=1µs, under resonance conditions.

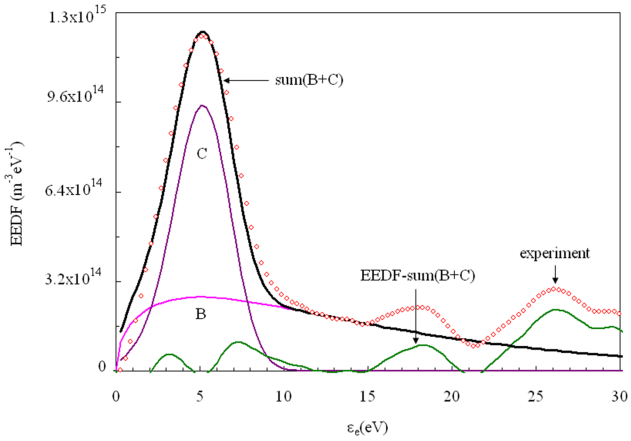

FIG. 10. Decomposition of EEDF in three main components; measurements are performed at low pressure at 1500W and at τ_s=10µs, i.e. τ_d=5µs, under resonance conditions.

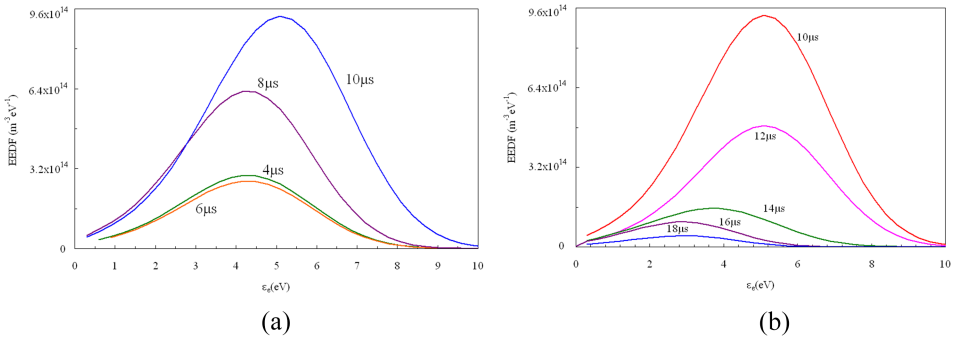

FIG. 11. a) Change of the low energy component until τ_s=10µs i.e τ_d=5µs after switching off; measurements are performed at P=0.38Pa and 1500W, under resonance conditions. b) Change of the low energy component from 10µs to 18µs; measurements are performed at P=0.38Pa and 1500W, under resonance conditions.

Using the standard functional fitting on EEDF profiles, we have studied the change of the components during the decay. Figures 11(a, b) and Figure 12 show the change of the low energy component (Fig 11a until τ_s=10µs and Fig 11b for τ_s>10µs) and intermediate energy component (Fig 12) for measurements performed at 0.38Pa and 1500W, under resonance conditions. In this last case the

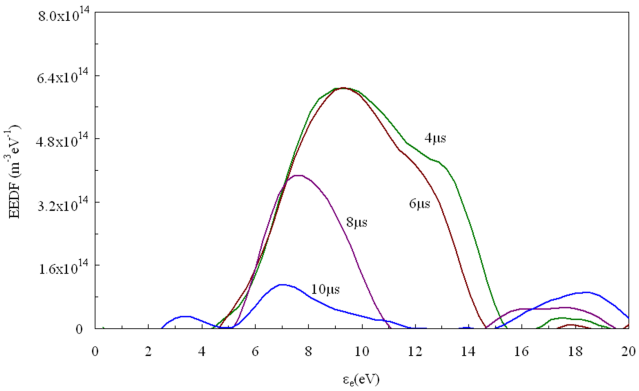

FIG. 12. Change of the intermediate energy component until τ_s=10µs i.e τ_d=5µs after switching off; measurements are performed at P=0.38Pa and 1500W, under resonance conditions.

Maxwell-Boltzmann component is very low compared to the two other ones and it cannot be studied like the two other components. It can be seen that above τ_s=5μs (τ_d=0μs, start of the decay), the intermediate energy component decreases up to about τ_s=10μs whereas the low energy component simultaneously increases. Then, the low energy component decreases and disappears at about τ_s=18μs (see Fig 11b), when the intermediate energy component is vanished. These results confirm the previous qualitative observations done for results shown Figure 6.

As previously explained, the incoming power decreases exponentially versus time after switching off. The signal is 60% of the initial signal at 5μs after switching off (τ_s=10μs) and 10%, at 10μs after switching off (τ_s=15μs). The time of the decay (12μs) measured for the high energy component (Maxwell-Boltzmann) and observed under off resonance conditions (see Figure 7), is similar to the time of the exponential decay observed at the incoming power. These two decay times could be correlated to the microwave resonance within the reactor. The microwave energy is stored within the plasma in the cavity with a high quality factor.

The intermediate energy component, observed under resonance conditions, only stands for τ_d=5μs. As shown Figure5 a large part of the applied power is absorbed, resulting in effective electron heating, ionization or dissociation. Transverse diffusion is absent because of magnetic confinement and thus the major loss is the outward expansion along the magnetic field. This could explain the observed electron density decay time (around 5μs) of the intermediate component after the power has stopped. Assuming an ion energy ranging from 0.1eV to 1eV, the expansion velocity ranges from $3x10^3$m/s to 10^4m/s and for a length of about 5cm (half length of the reactor cavity), the expansion time is between 5μs to 10μs as observed. So, in this assumption, during these first 5μs, the decay would be controlled by the outward expansion, from the centre where the plasma is heated and the pressure is higher to the wall where it is colder. Then, for larger time (τ_d>5μs), the outward expansion effect decreases, the plasma is more homogeneous and the electron decay results of recombination processes rather than the slow longitudinal diffusion (see below). However, it is worth noting that because of the high quality factor of the cavity, the incident power decreases slowly within the reactor, over more than 20μs. Consequently, the input power slowly decreases during these 20μs, the incident power is equal to 50% of the initial value 5μs after switching off. So the effect of the plasma expansion on the electron decay of the intermediate component is probably less important than expected. The reminiscence of this component during 5μs certainly depends on the plasma expansion but also it could be partly due to a resonant standing wave produced within the reactor and vanishing with electron density decreasing. Different electron waves can propagate within the cavity when a magnetic field is applied, depending on plasma parameters, on the magnetic field intensity and orientation in the cavity and on boundary conditions on the reactor wall.[23] A kinetic model should be more appropriated to explain this complex phenomenon concerning the intermediate component.

The low energy component first increases with decreasing intermediate energy component (until τ_s= 10μs), then decreases when the intermediate energy component is vanished.

We have studied the decays of the low energy component under different experimental conditions to explain this behaviour.

Figure 13 shows two examples of electron density decays, corresponding to the low energy component versus time after switching off. These results are obtained under resonance conditions at low and high pressure, at 1500W, and when the intermediate energy component is vanished. The electron density is calculated integrating over the low energy component of the distribution. The density decreases exponentially versus time from τ_s=8μs up to about 20μs. This is due to the recombination of electrons in the plasma bulk, and to the electron diffusion to the reactor wall. The balance equation can be written:

$$\frac{dn_e}{dt} = -kn_e n_{H2} - D\nabla^2 n_e. \tag{9}$$

The first part of the right side of this equation is the recombination of electron and the second part is the electron diffusion which is the sum of the radial and longitudinal diffusion within the reactor. The magnetic field has no effect on the longitudinal component of the electron velocity, and consequently on the longitudinal diffusion coefficient ($D_{//}$). However the radial diffusion coefficient ($D_{\perp}$) decreases

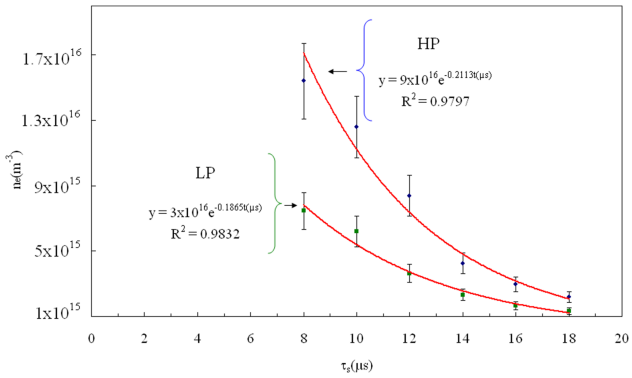

FIG. 13. Electron decay versus time, for the low energy component. Measurements are performed at 1500W at 0.38Pa (LP) and 0.62Pa (HP), respectively, under resonance conditions.

with magnetic field increasing. The diffusion transfer is anisotropic and the radial diffusion transfer can be neglected compared to the longitudinal diffusion transfer ($\frac{D_\perp}{D_{//}} = 1x10^{-5}$) at B=0.087T.

Assuming a 1D simple model with no spatial variation of the diffusion coefficient and considering elastic collisions between H_2^+ and neutral as the dominant collision process. Particles of opposite charges diffuse together due to their interaction and the global diffusion transfer depends on the ambipolar diffusion coefficient.[24] Because of the low ion mobility compared to the electron mobility, the ambipolar diffusion coefficient is given by

$$D_a = D_i(1 + \frac{T_e}{T_i}) \tag{10}$$

Where, D_i is the ion diffusion coefficient and T_e/T_i is electron/ion temperature ratio (i.e. mean electron/mean ion energy ratio within the plasma). assuming that the mean electron energy is 10eV, the mean ion energy ranges from 0.1eV to 1eV, the ambipolar diffusion coefficient D_a ranges from 738 m^2s^{-1} to 6775 m^2s^{-1} at 0.38Pa.

The effect of the diffusion on the electron decay during "off" time can be determined considering only the diffusion part in the balance equation (2). When the probe is located in the middle of the reactor on the z-axis, assuming a symmetric system of dimension 2L equal to the reactor length (93mm), the electron density at the probe tip decreases exponentially versus time, according to,

$$n_e = n_{e0}\exp(\frac{-t}{\tau}). \tag{11}$$

Where τ is the characteristic diffusion time given by,[6]

$$\tau = \left(\frac{2L}{\pi}\right)^2 \Big/ D_a. \tag{12}$$

It ranges from 0.1µs to 1.2µs. These values are one to two orders of magnitude lower than the decay time measured for the low energy component (8µs to 10µs). This simple calculation shows that the electron decay time is not due to the electron diffusion transfer in our experiments. It can be explained assuming homogeneous plasma within the reactor. So, there is no electron density gradient along the longitudinal axis after switching off and the electron diffusion transfer is not efficient.

By neglecting the diffusion part in the balance Equation (9), the electron decay is only due to the recombination process. It can be described by a global process proportional to hydrogen density. So, the electron density can be written:

$$n_e = n_{e0}\exp(-kn_{H2}t). \tag{13}$$

This equation describes the electron density decay versus time as shown on Figure 13 and the reaction rate constant can be calculated using the slope of the semi-logarithm representation, $\ln(n_e)=f(t)$.

Figure 14 shows the reaction rate constant measured versus incoming microwave power. The measurements have been performed using the experimental decay of the low energy component versus

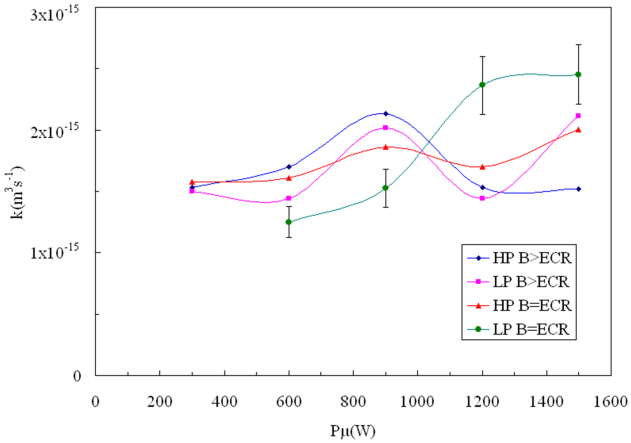

FIG. 14. Reaction rate constant value measured at 0.38Pa (LP), 0.62Pa (HP) versus incoming power, under resonance ($B=B_{ECR}$) and off resonance ($B>B_{ECR}$) conditions.

time under different experimental conditions which are low and high pressure, under resonance and off resonance conditions. It can be seen that the reaction rate constant value ranges between $1.1x10^{-15}m^3s^{-1}$ and $2.7x10^{-15}m^3s^{-1}$.

According to de Graaf et al[25] the recombination of electrons in hydrogen plasma proceeds in two steps: First there is a charge transfer between H_2 vibrational excited ($v\geq4$) and protons,

$$H_2(v \geq 4) + H^+ \longrightarrow H_2^+ + H. \quad (a)$$

Second, there is the recombination between electrons and molecular ions H_2^+. This reaction can be a direct recombination with dissociation because of energy excess,

$$H_2^+ + e \longrightarrow H + H \quad (b)$$

Or a recombination after charge transfer producing H_3^+,

$$H_2^+ + H_2 \longrightarrow H_3^+ + H \quad (c)$$

and a dissociative recombination of H_3^+,

$$H_3^+ + e \longrightarrow 3H \quad (d)$$

Or

$$H_3^+ + e \longrightarrow H_2(v,J) + H. \quad (e)$$

The reaction (d) is less probable than (e). Thus, two electron recombination mechanisms are possible in hydrogen plasma, the first is (a), (b) and the second (a),(c),(e). According to Phelds,[26] the dominant cross section for the low energy collision of H_2^+ in H_2 corresponds to the reaction (c). At a relative kinetic energy ranging from 0.1eV to 1eV, the cross section ranges from $78x10^{-20}m^2$ to $22.7x10^{-20}m^2$ which corresponds to reaction rate constants ranging from $1.7x10^{-15}m^3s^{-1}$ to $2.2x10^{-15}m^3s^{-1}$, respectively. These values are of the same order as the values calculated in the case of the Langevin charge transfer approximation ($2.5x10^{-15}$ m^3s^{-1}) and they are close to the values measured in the present work. This suggests that the charge transfer process (c) is the lowest step of the global recombination process under all experimental conditions investigated in this work. The electron recombination in the reactor is the mechanism (a), (c), (e). The energy excess due to the recombination is dissipated in translation or vibration energy by H_2 or H atom. These results show that during "off" time under resonance conditions, the low energy component first increases because of the decay of the intermediate energy component standing for 5 μs after the discharge is switched off, and second it decreases when the intermediate energy component is vanished. The low energy component decay is mainly due to the recombination process limited by the charge transfer producing H_3^+ ion and not to the electron diffusion transfer. The results show that the recombination process is not sufficient to balance the decrease of the intermediate energy component up to τ_s=10μs.

Under off resonance conditions, the high energy component (Maxwell-Boltzmann) stands longer than the intermediate energy component. A first increase of the low energy component is observed up to 8μs after switching off probably because of the excess of electrons produced during the first step of the high energy component decay. Then both components decrease simultaneously when the electron recombination process balances the decrease of the high energy component, and they vanish at τ_s>20μs.

IV. CONCLUSION

This work is devoted to the study of the afterglow observed for 20μs after switching off. Standard fitting methods have been used to study the different components of the EEDF profiles which are measured in the middle of the reactor. We briefly recall the method used to determine the EEDF from probe characteristics measured in H_2 magnetoplasma, taking into account the effect of the magnetic field on the electron current collected by the probe. We give new information concerning the energy relaxation length at low electron energy (<1eV) and we compare the Arslanbekov theory used in this work to the earlier Dote theory.

Three main components are observed:

The first corresponds to low energy electrons (ε_e<10eV) which is due to inelastic collisions i.e. between electrons and heavy particles. Its decay depends on the electron recombination process within the plasma, which remains the same under any experimental conditions investigated (at low and high pressure, at power ranging from 300W to 1500W, under and off resonance conditions). The rate constant value ranges from $1.1x10^{-15}$ to $2.7x10^{-15}$ m^3s^{-1}. It is characteristic of a charge transfer process, $H_2^+ + H \rightarrow H_3^+$ which limits the electron recombination rate.

The second intermediate energy component corresponding to electron energies ranging from 5 to 15 eV is mainly observed at low pressure and power larger than 600W under resonance conditions. It stands for 5μs after switching off. Meanwhile the low energy component increases because of low energy electrons produced by the intermediate energy component decrease and staying confined within the reactor bulk. Then the low energy component decreases when the recombination process, limited by the charge transfer, balances the electron excess.

The intermediate energy component standing for 5μs, can be observed even at power lower than 600W, during "off" time. The decay of this component is probably due to the plasma expansion due to the plasma heating. However, because of the high quality factor of the cavity, the incoming power is not immediately stopped after switching off and incoming power stands for about 25μs. So the plasma outward expansion effect is probably not as important as expected and other phenomena could act on the component decay (resonant standing wave decay for example). An electron kinetic model is necessary to study this intermediate component behavior during the decay.

The third high energy component is a Maxwell-Boltzmann distribution and corresponds to the EEDF tail. This hot-electron component is mainly observed under off resonance conditions and is partly hidden by the intermediate energy component under resonance conditions. It is observed for 15μs to 20μs after switching off. The reminiscence of this component during "off" time can be correlated to the remaining incoming power which vanishes for about 20μs to 25μs after switching off.

[1] S. Gammino, L. Celona, G. Ciavola, F. Maimone, and D. Mascali, Rev. Sci. Instrum. **81**, 02B313 (2010).
[2] J. Pelletier and A. Anders, IEEE Trans. Plasma Sci. **33**, 1944–1959 (2005).
[3] R. W. Boswell, O. Sutherland, C. Charles, J. P. Squire, F. R. Chang Dias, T. W. Glover, V. T. Jacobson, D. G. Chavers, R. D. Bengtson, E. A. Bering, R. H. Goulding, and M. Light, Phys of Plasmas **11**, 5125–5129 (2004).
[4] D. A. Glocker, J. Vac. Sci. Technol. A. **11**, 2989 (1993).
[5] A. Belkind, A. Freilich, and R. Scholl, J. Vac. Sci. A. **17**, 1934 (1999).
[6] H. Bäcker, J. W. Bradley, P. J. Kelly, and R. D. Arnell, J. Phys. D: Appl. Phys. **34**, 2709–2714 (2001).
[7] I. Izotov, D. Mansfeld, V. Skalyga, V. Zorin, T. Grahn, T. Kalvas, H. Koivisto, J. Kompula, P. Peura, O. Tarvainen, and V. Toivainen, Phys. Plasmas **19**, 122501 (2012).
[8] J. L. Jauberteau, I. Jauberteau, D. Cortázar, and A. Megía-Macías, Phys. Plasmas **23**, 033513 (2016).
[9] K. Takahashi, S. Takayama, A. Komuro, and A. Ando, Physical Review Letters **116**, 135001 (2016).
[10] G. Melin, F. Bourg, P. Briand, J. Debernardi, M. Delaunay, R. Geller, B. Jacquot, P. Ludwig, T. N'Guyen, L. Pin, M. Pontonnier, J. Rocco, and F. Zadworny, Rev. Sci. Instrum. **61**, 236 (1990).
[11] K. Langhein, 12th International Workshop on ECR ion Sources, Ricken, Japan 25–27 (1995).

[12] O. D. Cortázar, A. Megía-Macías, and A. Vizcaíno-de-julián, Rev. Sci. Instrum. **84**, 093301 (2013).
[13] O. D. Cortázar, A. Megía-Macías, O. Tarvainen, T. Kalvas, and H. Koivisto, Review of Scientific Instruments **87**, 02A704 (2016).
[14] O. D. Cortázar, A. Megía-Macías, and A. Vizcaíno-de-julián, IEEE Trans. Plasma Sci **40**, 3409 (2012).
[15] R. R. Arslanbekov, N. A. Khromov, and A. Kudryavtsev, Plasma Source Sci. Technol. **3**, 528–538 (1994).
[16] T. K. Popov, P. Ivanova, M. Dimitrova, J. Kovačič, T. Gyergyek, and M. Čerček, Plasma Sources Sci. Technol. **21**, 025004 (2012).
[17] F. Jauberteau and J. L. Jauberteau, Applied Mathematics and Computation **215**, 2283–2297 (2009).
[18] U. Kortshagen, Phys. Rev E **49**(5), 4369–4380 (1994).
[19] H. Tawara, Y. Itikawa, H. Nishimura, and M. Yoshino, J. Phys. Chem. Ref. Data **19**(3), 617–636 (1990).
[20] F. F. Chen, "Lecture notes on Langmuir probe diagnostics, mini-course on plasma diagnostics," IEEE-ICOPS meeting, Jeju, Korea, June 5, (2003).
[21] Vasil'Eva, High-Temperature **12**, 405 (1974).
[22] T. Dote, H. Amemiya, and T. Ichimiya, Jpn. J. Appl. Phys. **3**(12), 789–796 (1964).
[23] A. Megía-Macías, O. D. Cortázar, and A. Vizcaíno-de-julián, Rev. Sci. Instrum. **85**, 033310 (2014).
[24] F. F. Chen, *Introduction to Plasma Physics and Controlled Fusion*, 2th Edition, Vol:1, Plenum Press, New York (1984).
[25] M. J. de Graaf, R. Severens, R. P. Dahiya, M. C. van de Sanden, and D. C. Schram, Phys. Rev. E **48**, 2098–2102 (1993).
[26] V. Phelds, J. Chem. Phys. Ref. Data **19**, 653–675 (1990).